AIP | Journal of Applied Physics

Optimization of the scattering design in photoelectrode for dye-sensitized solar cells by theoretical simulation

X. Z. Guo and W. Z. Shen

Citation: J. Appl. Phys. **114**, 074310 (2013); doi: 10.1063/1.4818438
View online: http://dx.doi.org/10.1063/1.4818438
View Table of Contents: http://jap.aip.org/resource/1/JAPIAU/v114/i7
Published by the AIP Publishing LLC.

Optimization of the scattering design in photoelectrode for dye-sensitized solar cells by theoretical simulation

X. Z. Guo[1] and W. Z. Shen[1,2,a)]
[1]*Department of Physics and Astronomy, Institute of Solar Energy, Shanghai Jiao Tong University, 800 Dong Chuan Road, Shanghai 200240, People's Republic of China*
[2]*Laboratory of Condensed Matter Spectroscopy and Opto-Electronic Physics, and Key Laboratory of Artificial Structures and Quantum Control (Ministry of Education), Department of Physics and Astronomy, Shanghai Jiao Tong University, 800 Dong Chuan Road, Shanghai 200240, People's Republic of China*

(Received 28 April 2013; accepted 30 July 2013; published online 20 August 2013)

Light scattering design in dye-sensitized solar cells (DSCs) is important for improving the light harvesting efficiency. In this paper, we present a Monte Carlo simulation model of photon propagation in DSCs and demonstrate its effective usage in photoelectrode film design. With this model, scattering design in N719 dye sensitized photoelectrode is investigated and optimized. Effects of particle size, particle concentration, layer structure, as well as specific surface area are examined. Simulations demonstrate that multi-layer films with gradually increased scattering particles are superior to single- or double-layer ones, since such a film structure can improve light absorption in long wavelength region and suppress light loss due to back-scattering simultaneously. Light harvesting efficiency of cell can be further improved by optimizing the size and specific surface area of scattering particles. Our results are in good agreement with the reported experimental ones, proving the reliability and validity of this simulation approach. [http://dx.doi.org/10.1063/1.4818438]

I. INTRODUCTION

Absorption of incident light is the first step in photoelectric conversion process of solar cells, and the dye-sensitized solar cell (DSC)[1–4] emerged as a low-cost photovoltaic device is no exception. To achieve high performance especially large short-circuit current density (*J*sc), efficient light harvesting is essential. In the case of DSCs, the incident photons are absorbed by dye molecules attached to the surface of TiO_2 nanocrystalline films. The most commonly employed dye represented by N719 can absorb light with the wavelength up to 800 nm, but its extinction coefficients above 650 nm are too low to catch photons efficiently.[5] Although the light harvesting efficiencies (η_{LHE}) at these wavelengths can be improved with thicker photoelectrode, the thickness of TiO_2 nanocrystalline film cannot be increased at will without affecting its mechanical properties, increasing charge recombination or raising series resistance of the cell. Therefore, it is desirable to enhance light absorption for a given film thickness by optical design. Reported theoretical and experimental results proved that η_{LHE} in red region could be improved by the light scattering of submicron particles either embedded in the nanocrystalline film or deposited on it.[6–11] In fact, virtually all DSCs that exhibit above 11% efficiency employ photoelectrode films with scattering structures.[12–15]

Although large particles incorporated in the film can enhance light absorption, this enhancement may be offset by the light loss due to back-scattering and by a lower dye concentration resulting from the reduction of specific surface area. Wang *et al*. have found that the performance of DSCs depended strongly on the light scattering design in TiO_2 film. Energy conversion efficiency of N719 dye-sensitized solar cell has been improved significantly by optimizing the film structure.[10] Their research is meaningful and valuable. However, the experimental optimization of scattering design in photoelectrode is targeted, namely it is carried out for a certain sensitizer. When switching to other kinds of sensitizers, such as organic dye or quantum dot, the optimal structure will inevitably need adjustment. Moreover, light harvesting is also influenced by the properties of TiO_2 nanocrystalline film (such as porosity, specific surface area, crystal structure, etc.) which may vary depending on the preparation method. As a result, experimental optimization of photoelectrode structure has to be redone whenever changing the sensitizer or improving the techniques. Researchers have to repeat the process of sample preparation and characterization several times spending a lot of time and effort. Besides, the quality of film affected by preparation experience may impact on the assessment of film structure. Computer simulation with the advantages of convenient, efficient, and flexible can be applied to film structure design. More importantly, reliable theoretical simulations can provide guidance for the optimization of film structure and reduce workload.

Modeling photon propagation with Monte Carlo method is a flexible yet rigorous approach to simulating photon transport in DSC photoelectrodes.[16,17] Compared with many-flux method,[18] no parameters involved in Monte Carlo method need to be determined empirically from experimental transmittance or reflectance data. Therefore, this method can be used to simulate the light harvesting properties of DSCs before practical experiments, and it is more suitable for the theoretical design of scattering structure.

a)Electronic mail: wzshen@sjtu.edu.cn

In this paper, we present a Monte Carlo simulation model of photon propagation in DSCs and investigate the optical performance of N719 dye sensitized photoelectrode films with different scattering structures. Effects of particle size, concentration, layer structure, as well as specific surface area are examined. Quantitative analysis of light loss due to back-scattering, average optical path length within the film, and light harvesting efficiency is provided. Calculated results are compared with the reported experimental ones to examine the reliability of our simulation approach.

II. THEORETICAL MODEL

Photoelectrodes with single-, double-, or multi-layer structures were analyzed. Schemes of these different photoelectrodes are drawn in Fig. 1. According to the content, all film layers can be divided into three types: transparent layer, mixed layer, and scattering layer. Transparent layer contains no large particles, and the diameter of TiO_2 nanoparticles is supposed to be 20 nm. In mixed layer, small and submicron TiO_2 particles are mixed uniformly. The morphology of mixed layer, in additional to the region occupied by submicron particles, is assumed to be the same as that of transparent layer. Scattering layer consists only of submicron TiO_2 particles. In this simulation, the total film thickness is 15 μm for all photoelectrodes studied.

A. Optical modeling

Based on the theoretical model proposed by Niklasson *et al.*,[19] nanocrystalline film can be treated as an apparently non-scattering medium with an effective refractive index. Thus, multiple light scattering of only submicron particles is taken into account. In this paper, Monte Carlo method is employed to simulate the trajectory of 10^6 photons that enter different DSCs under consideration. Similar approaches have also been used by Usami[16] and Gálvez *et al.*[17] to study the contribution of light confinement and the combined effect of light harvesting and electron collection in DSCs.

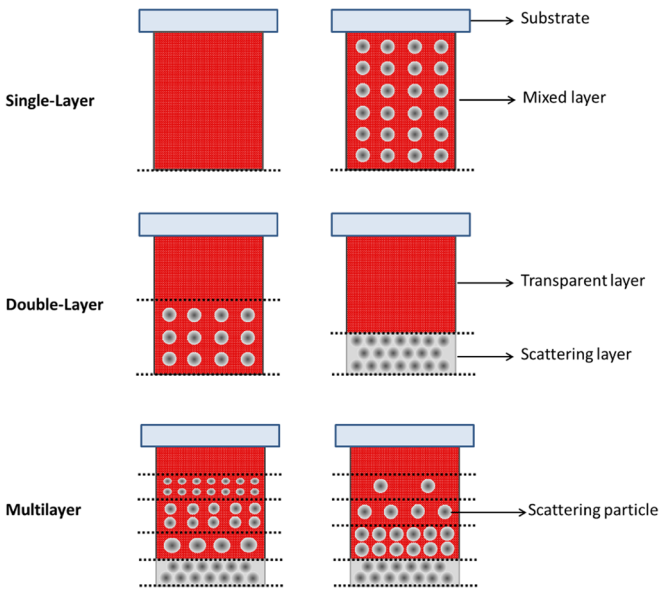

FIG. 1. Schematic film structures of studied photoelectrodes.

The trace simulation of a photon is carried out with the following steps. First, transmission length l, the distance traveled before experiencing either absorption or scattering, is calculated by the expression

$$l = -\ln[r]/(\alpha_{abs} + \alpha_{sca}), \tag{1}$$

where r is a random number comprised in the range $0 < r \leq 1$, α_{abs} and α_{sca} are the absorption and scattering coefficients, respectively. Second, absorption or scattering is determined by a second random number r'. If $r' \leq \alpha_{sca}/(\alpha_{abs} + \alpha_{sca})$, the photon is scattered, and the scattering angle is determined by a third random number r''. Then, the simulation returns to the first step. If $r' > \alpha_{sca}/(\alpha_{abs} + \alpha_{sca})$, the photon is absorbed. The simulation is over when the incident photon is absorbed or goes out of the film.

In the photoelectrode film, photons can be absorbed by electrolyte as well as N719 dye. However, only the light harvesting occurring at dye molecules contributes to the photocurrent. In addition, optical loss caused by electrolyte is small and the differences between different DSCs under consideration can be ignored. Therefore, α_{abs} herein is simplified to the absorption coefficient of dye in the film and can be expressed as

$$\alpha_{abs} = \varepsilon c, \tag{2}$$

where ε is the molar extinction coefficient of dye and c is the adsorption amount of dye per unit volume of the film. Since c is approximately proportional to the specific surface area of photoelectrode film, $c = c_0 S'/S_0$, where c_0 is the adsorption amount of dye per unit volume of transparent layer, S_0 and S' are the specific surface area of transparent layer and mixed (or scattering) layer, respectively. We assume that all particles are spherical and disconnected with each other, then the specific surface area equals to the total surface area of all particles per unit volume.

In this simulation, the angle dependence of scattering intensity is assumed to be that of a spherical TiO_2 particle and calculated with three-dimensional finite-difference time-domain (FDTD) method. A commercial FDTD software package, FDTD Solutions, provided by Lumerical Solutions, Inc. is used. The scattering cross-section of a single particle (σ) is also calculated with FDTD method. The σ value corresponds to the total power of far-field scattered light in all directions divided by the incident light intensity. The scattering coefficient α_{sca} is the fraction of light scattered per unit distance in the film. For a mixed layer containing N kinds of scattering particles, α_{sca} is essentially the scattering cross-sectional area per unit volume, expressed as

$$\alpha_{sca} = \sum_{k=1}^{N} \sigma_k \rho_k, \tag{3}$$

where σ_k is the scattering cross-section of particle k, and ρ_k is the number of particle k per unit volume (k = 1, 2,…, N). Formula (3) is applicable only when the volume fraction of large particles is low ($\leq$30%). In the scattering layer, the volume fraction of large particles is about 50%, and the

cancellation of multipoles cannot be ignored. For this case, Gálvez *et al*. have taken an approximation and set the scattering coefficient α_{sca} as a constant. Their calculated results were in excellent agreement with the reported experimental ones.[17] In this paper, similar approximation is used, i.e., the α_{sca} of scattering layer is set as 2 μm^{-1}.

Using this model, we obtained the light harvesting efficiency η_{LHE} and the electron generation profile $g(x, \lambda)$ for all the cells studied. The spectral region is 400 nm–800 nm; the spectral and spatial resolution considered are $\Delta\lambda = 10$ nm and $\Delta h = 100$ nm, respectively. The molar extinction coefficient of N719 dye (ε) and its adsorption amount per unit volume of transparent layer (c_0) were extracted from reported data in Ref. 10. Besides, we neglected the specular reflectance at the interfaces to simplify the calculation, which will cause underestimation of η_{LHE}. Since similar deviations are introduced for different photoelectrode films and the underestimation of J_{SC} is small, we inferred that the specular reflection at the interfaces can be omitted without influencing the optimization of scattering structure.[20]

B. Electrical modeling

For most high-efficiency DSCs, Jsc is proportional to the incident light intensity, so it can be calculated by the overlap integration of global AM (standard global air mass) 1.5 solar emission spectrum and the photocurrent action spectrum,[21] expressed as

$$J_{SC} = q\int [1 - R(\lambda)]F(\lambda)IPCE(\lambda)d\lambda, \tag{4}$$

where q is the electron charge, λ is the wavelength, F is the incident photon flux density, R is the incident light loss due to the absorption and reflection by conducting glass (its value was extracted from reported data in Ref. 22), and IPCE is the incident monochromatic photon-to-electron conversion efficiency. The IPCE value corresponds to the photocurrent density produced in the external circuit under monochromatic illumination of the cell divided by the photon flux that strikes the cell. IPCE is determined by three partial efficiencies: light harvesting efficiency (η_{LHE}), electron injection efficiency (η_{inj}), and charge collection efficiency (η_{CC}), expressed as

$$IPCE(\lambda) = \eta_{LHE}(\lambda)\eta_{inj}(\lambda)\eta_{CC}(\lambda). \tag{5}$$

In fact, light scattering in the photoelectrode film can be assumed to have no effect on η_{inj}, which is almost unity for high performance DSCs.[23–26] So IPCE can be simplified as the product of η_{LHE} and η_{CC}. With standard diffusion model and linear recombination assumption, the steady-state solution for η_{CC} at short-circuit condition can be written as[27,28]

$$\eta_{CC}(\lambda) = \frac{1}{\cosh(d/L)} \times \frac{\int_0^d g(x,\lambda)\cosh[(d-x)/L]dx}{\int_0^d g(x,\lambda)dx}, \tag{6}$$

where d is the photoelectrode film thickness, g is the local electron generation rate, and L is the electron diffusion length. Depending on the illustration intensity, the value of L can be tens of microns for high performance DSCs.[29–31] In this simulation, the value of L is fixed as 30 μm.

It should be noted that Eq. (6) is established under the following assumptions: (1) Electron recombination is linear with the electron density and (2) electron diffusion coefficient and lifetime are independent of the electron density and position in the photoelectrode film. In typical DSCs, these two assumptions are not accurate. The electron diffusion length L cannot be defined as a constant parameter but needs to be discussed in terms of the so-called small perturbation diffusion length λ_n.[32] However, it has been found by Barnes and O'Regan that the linear model could give very similar results for the η_{CC} and IPCE as the nonlinear model even at short-circuit condition.[33] Moreover, the value of L is much larger than the thickness of photoelectrode film in our simulation, and η_{CC} is nearly independent of the spatial distribution of light absorption (see Sec. III B). We inferred that the errors caused by the linear model will not impact the theoretical optimization of scattering design.

III. RESULTS AND DISCUSSION

A. Scattering coefficient and angle dependence

The size of submicron TiO_2 particle has a great impact on its scattering cross-section σ, as shown in Fig. 2(a). With the diameter increasing from 200 nm to 500 nm, σ of the particle increases significantly, especially in the long wavelength region. For example, at $\lambda = 700$ nm, σ of TiO_2 particles with diameter of 200, 300, 400, and 500 nm are 0.023, 0.142, 0.411, and 0.789 μm^2, respectively. However, when the weight fraction of the scattering particles (W) is fixed, the particle number per unit volume, ρ, decreases with the increasing of diameter. As a result, the increase in σ is offset when calculating the scattering coefficient α_{sca} [Fig. 2(b)]. With the particle diameter increasing from 200 nm to 500 nm, the average values of α_{sca} are 0.813601, 1.152818, 1.137808, and 1.020516 μm^{-1}, respectively. Besides, it can be seen that the maximum value of α_{sca} shifts to longer wavelength and the scattering intensity in long wavelength region increases with particle size.

Figure 3 displays the angle distribution of scattering intensity for a single spherical TiO_2 particle embedded in TiO_2 nanocrystalline film. The particle diameter is 200 nm–500 nm, and the total intensity in all directions is normalized. The results indicate that most scattered light goes forward, namely the scattering angle $\theta < 90°$ (θ is defined as the angle between incoming and outgoing direction of light). For a TiO_2 particle with 500 nm diameter, more than 90% scattered light has a small scattering angle ($\theta < 45°$). As the particle size decreases, the forward scattering intensity with large angle increases significantly, and the proportion of backscattered light also shows a slight increase.

B. Single-layer DSCs

Photoelectrode films with a single mixed layer were simulated first. These films are divided into four groups according to the scattering particle size. In each group, the

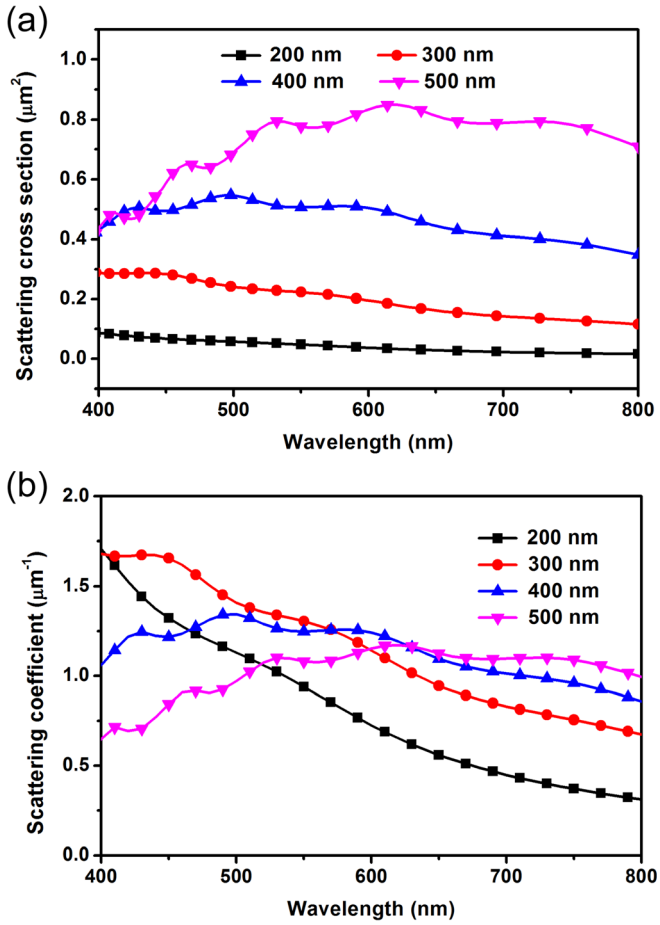

FIG. 2. Wavelength dependence of (a) scattering cross-section of a single submicron TiO_2 particle in nanocrystalline film and (b) scattering coefficients of photoelectrode films with mono-size scattering particles of 20% weight fraction. The diameters of submicron TiO_2 particles are specified in legends.

weight fraction of scattering particles, W, changes from 0% to 30%. Figure 4 illustrates the light harvesting efficiencies η_{LHE} of all these single-layer samples as a function of wavelength. It can be seen that the changes of η_{LHE} caused by W in each group exhibit similar characteristics: in short wavelength region (400 nm–550 nm), η_{LHE} decreases monotonically with the increasing of W; in long wavelength region (650 nm–800 nm), η_{LHE} firstly increases and reaches its maximum value when W is 15%–20%, then decreases slightly.

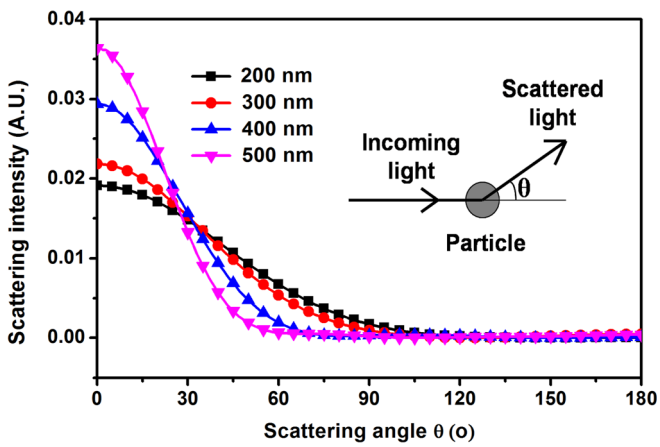

FIG. 3. Angle dependence of scattering intensities by a single submicron TiO_2 particle in nanocrystalline film calculated at $\lambda = 600$ nm. The total intensity in all directions is normalized and the diameters of the TiO_2 particles are specified in legends. Inset shows the definition of scattering angle θ.

The impact of scattering particles upon the film characteristics and photon propagation can be attributed to three aspects: (1) Submicron particle has smaller specific surface area, so the α_{abs} of mixed layer decreases compared with the transparent layer; (2) part of the incident photons will be reflected out of the film and lost due to back-scattering; and (3) for the other photons, light scattering caused by large particles will increase their optical path lengths as well as the probability of being absorbed. Apparently, changes in η_{LHE} depend on the combined effect of all three aspects, but only the last one is advantageous to improve light absorption. For the sake of conciseness, we refer to these three aspects as impact-I, II, and III, respectively.

The calculated results of single-layer samples at two representative wavelengths, 500 nm and 700 nm, are shown in Table I. These samples are named in the form of Sm-n ($m = 1, 2, 3, 4$; $n = 1, 2, 3$). Different m (n) values in the name correspond to different diameters (weight fractions) of scattering particles. S0 is the sample without scattering particles in the film. η_{R-Loss} is the percentage of light loss due to back-scattering, which can reflect the effect of impact-II. L_{AOP} is the average optical path length of photons within the film. At $\lambda = 500$ nm, the molar extinction coefficient of N719 dye is so high that almost all the incident photons are absorbed when no scattering particles exist (sample S0). However, with the introduction of scattering particles, η_{R-Loss} increases significantly. For all the single-mixed-layer samples, the sum of η_{LHE} and η_{R-Loss} approximately equals to 1, which indicates that the decrease of η_{LHE} in short wavelength region is mainly due to impact-II. The variation of L_{AOP} at $\lambda = 500$ nm is more complicated. On one hand, back-scattered photons tend to have shorter optical path. On the other hand, the optical absorption depth of photoelectrode film increases with W due to the reduction of α_{abs}. In long wavelength region, the molar extinction coefficient of N719 dye is much lower, so the effects of impact-III begin to emerge and dominate. After mixing large particles into the film, much more incident photons are absorbed owing to longer L_{AOP}. Consequently, η_{LHE} at $\lambda = 700$ nm increases with W at first, although the value of η_{R-Loss} is several times higher than that at $\lambda = 500$ nm. When W is too high (>20%), the negative effect of impacts I and II is bigger, and η_{LHE} decreases again.

The influence of scattering particle size can be obtained by comparing samples in different groups. When W is fixed, the scattering coefficient does not differ much as described in Sec. III A. However, with the increasing of particle diameter, average light scattering angle of a single particle decreases gradually. Thus, weaker back-scattering leads to the reduction of η_{R-Loss}. In short wavelength region, η_{LHE} increases monotonically with particle diameter. While in long wavelength region, the trend is no longer monotonous, and a maximum value of η_{LHE} is found when the diameter is 300 nm or 400 nm. The decline of η_{LHE} with bigger scattering particle can be explained as follows: (1) the absorption

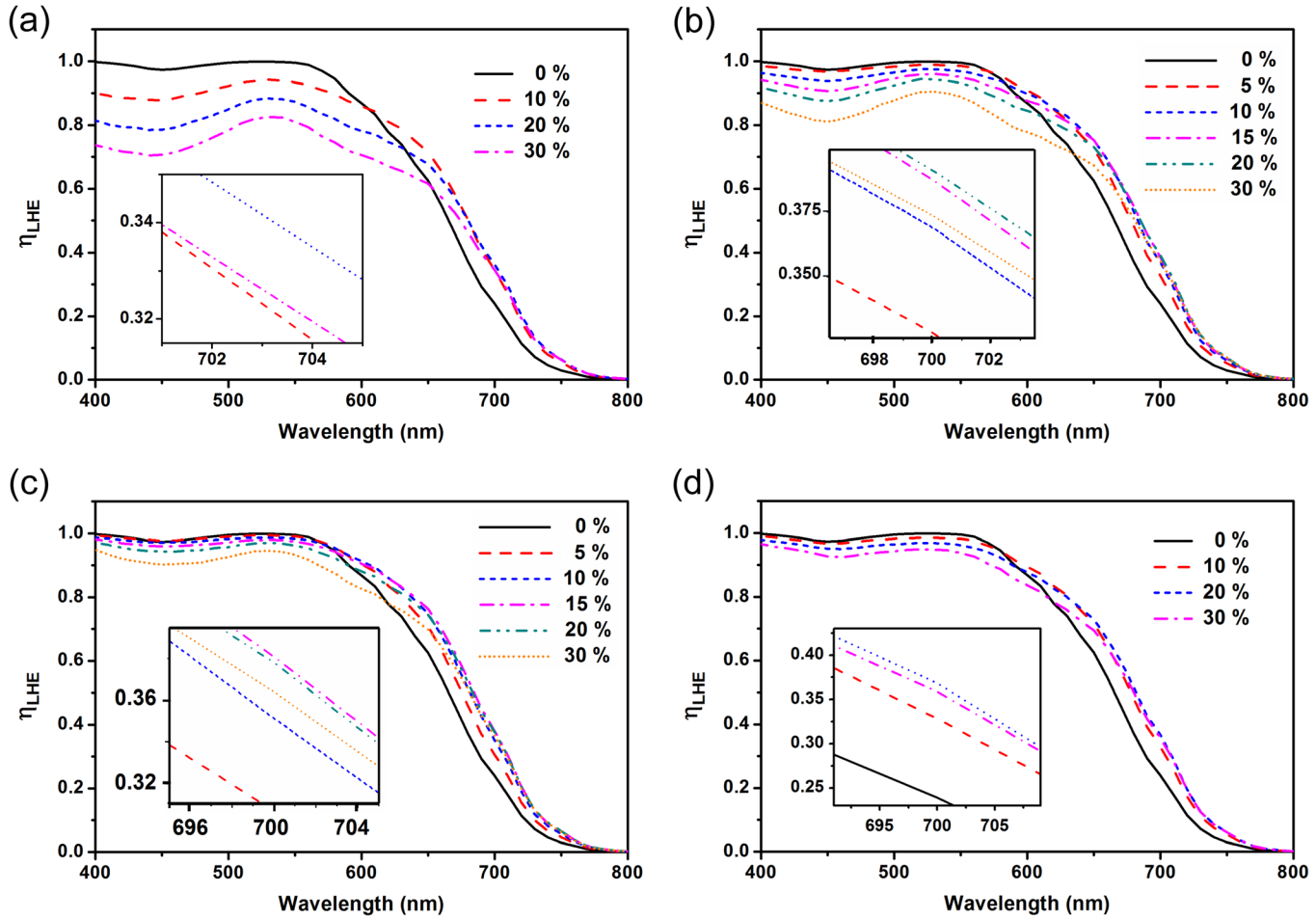

FIG. 4. Light harvesting efficiencies (η_{LHE}) of single-layer photoelectrode films as a function of wavelength. The diameters of scattering particles are (a) 200 nm, (b) 300 nm, (c) 400 nm, and (d) 500 nm. Inset is an expanded region around 700 nm.

coefficient α_{abs} decreases significantly and (2) the average scattering angle is too small that it is not conducive to improve L_{AOP}. We have also simulated single-layer samples in which scattering particles of different sizes were uniformly mixed together, but no obvious improvement has been found (not shown).

In addition to η_{LHE}, scattering particles also influence the electron generation function $g(x, \lambda)$. When light is

TABLE I. Simulation results of single-layer films with mono-size scattering particles.

			$\lambda = 500$ nm			$\lambda = 700$ nm			
Sample	D[a] (nm)	W[b] (%)	η_{LHE}	$\eta_{R\text{-}Loss}$	L_{AOP} (μm)	η_{LHE}	$\eta_{R\text{-}Loss}$	L_{AOP} (μm)	Jsc (mA/cm^2)
S0	/	/	0.995	0	2.84	0.239	0	13.14	15.04
S1-1	200	10	0.920	0.079	2.72	0.350	0.275	19.83	14.94
S1-2		20	0.856	0.144	2.61	0.366	0.433	21.68	13.91
S1-3		30	0.791	0.210	2.50	0.357	0.525	21.79	12.73
S2-1	300	10	0.966	0.034	2.85	0.369	0.237	21.27	15.74
S2-2		20	0.922	0.078	2.83	0.391	0.400	22.80	15.15
S2-3		30	0.875	0.125	2.81	0.369	0.503	22.89	14.21
S3-1	400	10	0.982	0.017	2.91	0.360	0.176	20.56	15.92
S3-2		20	0.961	0.039	2.95	0.385	0.332	23.02	15.81
S3-3		30	0.929	0.071	2.99	0.376	0.440	23.47	15.02
S4-1	500	10	0.982	0.016	2.92	0.334	0.174	19.14	15.66
S4-2		20	0.966	0.033	3.00	0.371	0.320	22.24	15.62
S4-3		30	0.945	0.055	3.08	0.370	0.426	23.11	15.15

[a]D is the diameter of scattering particles embedded in the film.
[b]W is the weight fraction of scattering particles in the film.

applied on the photoelectrode of DSC, the ground state electron of dye molecule is excited and subsequently transferred to the conduction band of TiO_2. The function $g(x, \lambda)$ describes the local electron generation rate per unit volume of nanocrystalline film, where x is the depth in the film. Since the excited state lifetime of dye (20 ns–60 ns) is much longer than the time of electron injection process (femtoseconds to picoseconds), it can be considered that there is no loss during this injection. As a result, $g(x, \lambda)$ is the same as the optical absorptance profile of the photoelectrode film. Figure 5 shows the $g(x, \lambda)$ of single-layer films with 300 nm scattering particles of different weight fractions. Two different wavelengths, 500 nm and 700 nm, were chosen to illustrate the effects corresponding to high and low absorption coefficient, respectively. The calculated results for photoelectrode film without scattering particles demonstrate exponential distribution, which is consistent with the Beer-Lambert law. With the increasing of large particles embedded in the film, more incident photons are absorbed near the substrate, and the average distance between photogenerated electrons and collecting contact gradually decreases. The drop of the average distance is bigger at $\lambda = 700$ nm than at $\lambda = 500$ nm. Gálvez *et al.*[17] have found that for DSCs in which electron diffusion length is shorter than film thickness ($L < d$), the shape and value of $g(x, \lambda)$ largely determine the charge collection efficiency η_{CC} and thus the overall performance. In our simulation, solar cells are of efficient charge collection ($L \gg d$), so the η_{CC} is nearly independent of the spatial distribution of light absorption with values between 0.91 and 0.99. Amount all the single-layer samples under consideration, the maximum J_{SC} appears when 400 nm TiO_2 particles are embedded in the photoelectrode film with a weight fraction of 10%–20%.

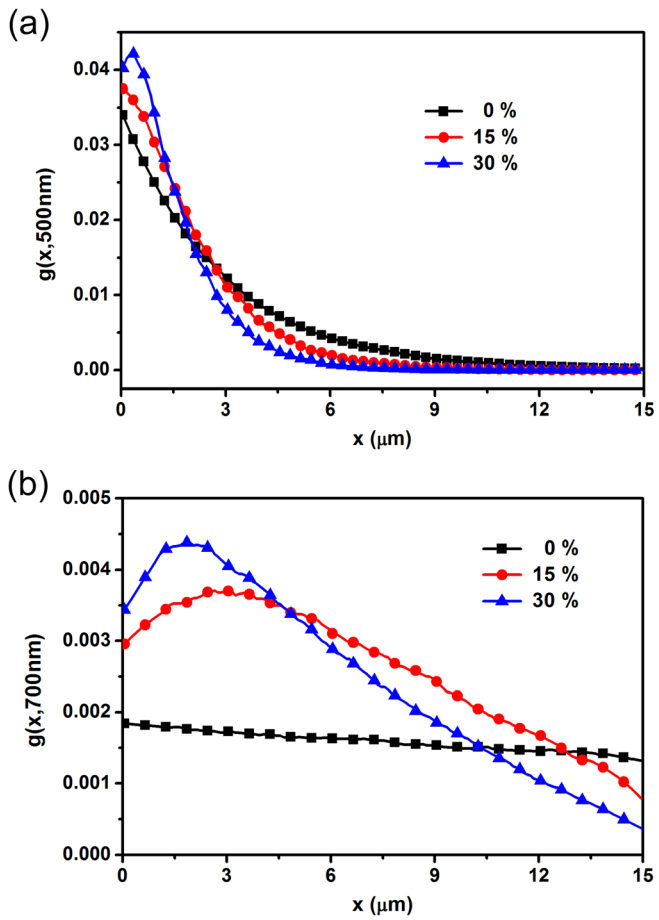

FIG. 5. Electron generation function [g(x, λ)] or spatial optical absorptance profile for single-layer films with 300 nm scattering particles calculated at (a) $\lambda = 500$ nm and (b) $\lambda = 700$ nm. The weight fractions of scattering particles are shown in legends.

C. Double-layer and multi-layer DSCs

In single-mixed-layer films, unfavorable back-scattering always occurs near the substrate. To reduce or suppress its influence, films with double-layer structures were designed by combining a transparent layer next to the conducting glass and a mixed or scattering layer on its top. In the double-layer films, photons "reflected" by the second layer will enter the first transparent layer again, thus part of them can be absorbed and reduce the light loss. Figure 6 displays the wavelength dependence of η_{LHE} calculated for two double-layer films, D1 and D2, with detailed structures shown in Table II. Scattering particles of 400 nm size were used for the simulation of double-layer structures due to their optimal effect for single-layer films. In fact, the size of scattering particles is exactly 400 nm for some reported DSCs with energy conversion efficiency above 10%.[12–14] The η_{LHE} of the single-layer film S3-2 is also drawn in Fig. 6 for comparison. Compared with S3-2, the η_{LHE} of D1 and D2 in short wavelength region are improved significantly. This remarkable improvement is persuasive evidence for the efficient suppression of back-scattering. More convincing evidence is provided by the reduction of η_{R-Loss} as shown in Table III. Unfortunately, the η_{LHE} of the two double-layer films above 650 nm (for D1) or 620 nm (for D2) are lower than that of S3-2. This decrease of η_{LHE} in long wavelength region should be explained by the weakened positive effect of light scattering (impact-III). Although the L_{AOP} of D2 calculated at $\lambda = 700$ nm is longer than that of S3-2, quite a long distance traveled by photons is in scattering layer, where the α_{abs} is extremely small. For further confirmation, a new parameter L'_{AOP} is defined as the relative optical path length in a film with absorption coefficient of α_0

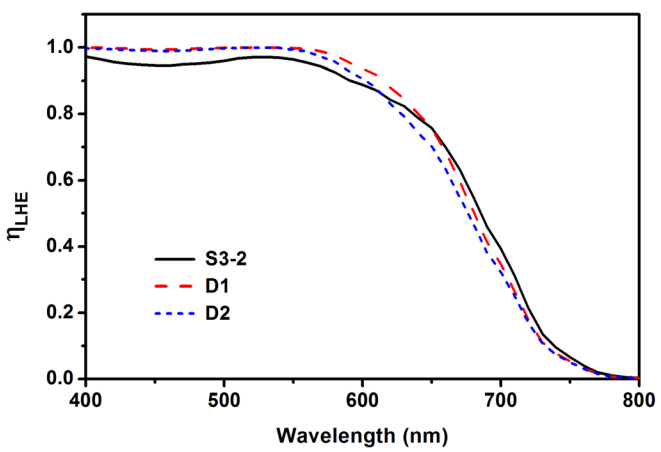

FIG. 6. Light harvesting efficiencies (η_{LHE}) of S3-2, D1, and D2 as a function of wavelength.

TABLE II. Detailed structures of double- and multi-layer films.

Sample	Layers[a]	Thickness (μm)	D[b] (nm)	W[c] (%)
D1	T	7	/	/
	M	8	400	20
D2	T	10	/	/
	S	5	400	100
T1	T	5	/	/
	M	2.5	400	10
	M	2.5	400	20
	M	2.5	400	30
	S	2.5	400	100
T2	T	5	/	/
	M	2.5	250	10
	M	2.5	300	20
	M	2.5	350	30
	S	2.5	400	100

[a]Layers are arranged according to the sequence beginning from the conducting substrate. T: transparent layer; M: mixed layer; S: scattering layer.
[b]D is the diameter of scattering particles embedded in the film.
[c]W is the weight fraction of scattering particles in the film.

$$L'_{AOP}(\lambda) = \sum_i \frac{l_i \alpha_{abs,i}(\lambda)}{\alpha_0(\lambda)}, \quad (7)$$

where l_i and $\alpha_{abs,i}$ are the transmission length and absorption coefficient for step i, respectively. It should be noted that $\alpha_{abs,i}$ is calculated by Eq. (2) and its value varies depending on the photon's position in the double-layer films. We make α_0 equals to the α_{abs} of S3-2, then L'_{AOP} at $\lambda = 700$ nm for D1 and D2 are 20.50 μm and 19.14 μm, respectively, both of which are much smaller than the L_{AOP} of S3-2 (23.02 μm).

Figure 7 shows the light absorptance profile or electron generation function $g(x, \lambda)$ of D1 and D2 at $\lambda = 700$ nm. Compared with sample S0 (also drawn in this figure), the electron generation in D1 is improved at each depth in the film. The improvements of $g(x, \lambda)$ in the transparent and mixed layer are attributed to the back-scattering from the mixed layer and the optical path increase in the mixed layer, respectively. Since scattering layer contains more large particles and has stronger back-scattering, the $g(x, \lambda)$ of D2 at $x \leq 10$ μm is even higher than that of D1. Contrary to the remarkable improvement of $g(x, \lambda)$ below 10 μm, the electron

TABLE III. Simulation results of double- and multi-layer films with detailed structures in Table II. T2′ and T2″ have the same structure as T2, while the surface areas of large particles incorporated in these two films are increased by 10-fold and 20-fold, respectively.

	$\lambda = 500$ nm			$\lambda = 700$ nm			
Sample	η_{LHE}	$\eta_{R\text{-}Loss}$	L_{AOP} (μm)	η_{LHE}	$\eta_{R\text{-}Loss}$	L_{AOP} (μm)	Jsc (mA/cm^2)
D1	0.9982	0.0001	2.88	0.345	0.156	19.71	16.13
D2	0.9967	0.0001	2.99	0.322	0.319	24.08	15.73
T1	0.9981	0.0003	2.89	0.389	0.306	25.39	16.41
T2	0.9990	0.0006	2.90	0.413	0.363	26.44	16.68
T2′	0.9994	0.0005	2.85	0.487	0.329	24.81	17.18
T2″	0.9994	0.0005	2.81	0.547	0.304	23.28	17.65

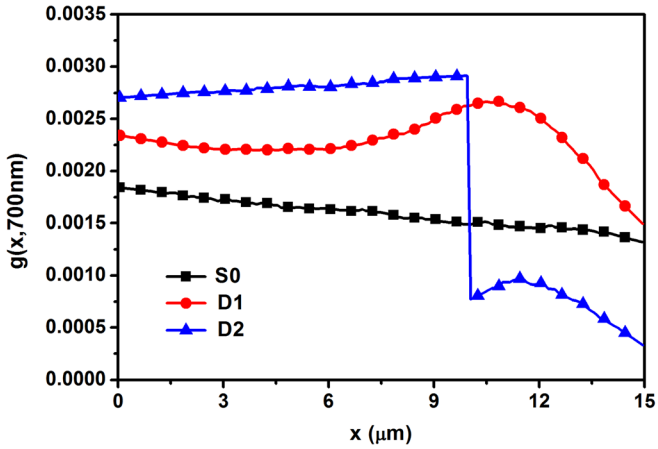

FIG. 7. Electron generation function [g(x, λ)] or spatial optical absorptance profile for S0, D1, and D2 calculated at $\lambda = 700$ nm.

generation of D2 at $x > 10$ μm decreases significantly. As described in Sec. II A, the adsorption amount of dye molecule per unit volume is approximately proportional to the specific surface area of photoelectrode film. Since the scattering layer in D2 ($x > 10$ μm) is composed of large TiO_2 particles, its specific surface area and adsorption amount of dye are rather small compared with the transparent layer ($x \leq 10$ μm). As a result, only a small amount of photons can be absorbed in the scattering layer, and thus $g(x, \lambda)$ of D2 decreases significantly at $x > 10$ μm. By integrating the light absorptance profile in the two double-layer films, it can be found that η_{LHE} of D1 at $\lambda = 700$ nm is higher than that of D2. In fact, D1 produces higher η_{LHE} in the whole visible region (see Fig. 6).

As described above, although the double-layer structure is better than the single-mixed-layer one in terms of back-scattering suppression, the positive light scattering effect in D1 or D2 is less efficient compared with S3-2, and the η_{LHE} in long wavelength region are lower. As a result, after changing the film structure from single-layer to double-layer, Jsc has little or no improvement (see Table III). In order to increase the Jsc of DSC, η_{LHE} should be enhanced in the entire visible region. Since α_{abs} decreases with the increasing of wavelength above 550 nm, incident photons with longer wavelength penetrate deeper into the film. It can be inferred that gradually increased scattering coefficient with the depth in the film may provide better optical characteristics. This can be realized by multi-layer structures. Here, we simulated two multi-layer samples, T1 and T2, with increased scattering particles. All the large particles in T1 are 400 nm in diameter, while the large particle size of T2 varied from 250 nm to 400 nm in different layers. The detailed structures are shown in Table II. Figure 8 depicts the wavelength dependent η_{LHE} of these two multi-layer films, where the spectrum of D1 is also appended for comparison. In order to demonstrate the differences between the three curves more clearly, only the η_{LHE} at 550 nm $\leq \lambda \leq$ 770 nm are shown in this figure. In fact, the η_{LHE} curves of T1, T2, and D1 below 550 nm almost coincide with each other and the values are almost unit, confirming that multi-layer films have similar effect as double-layer ones on back-scattering suppression.

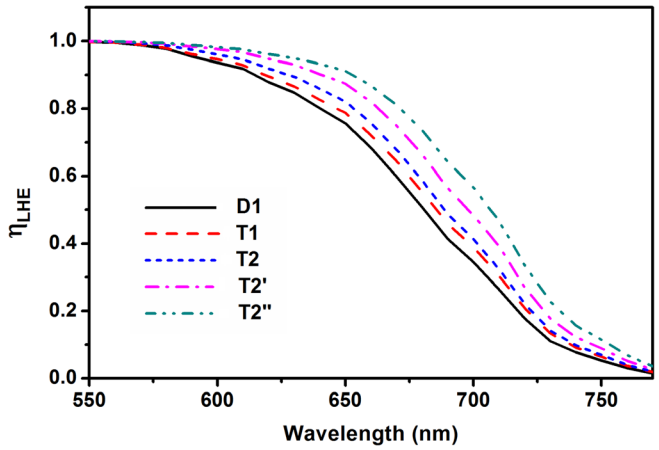

FIG. 8. Light harvesting efficiencies (η_{LHE}) of D1, T1, T2, T2′, and T2″ as a function of wavelength.

As shown in Figure 8, the η_{LHE} of both T1 and T2 are higher than that of D2 in the long wavelength region. These calculated results verified the above inference. In multi-layer films, the incident photons with wavelength of small α_{abs} penetrate deeper where more large particles are embedded. Thus, the strong light scattering in deeper layers lengthens these photons' optical path and improves the η_{LHE}. Compared with T1, the η_{LHE} of T2 are even higher. We believe that the main reasons include: (1) In the middle layers, the α_{abs} of T2 are higher due to the smaller size of scattering particles and (2) on one hand, bigger particles scatter more photons with long wavelength; on the other hand, smaller particles provide larger average scattering angle. With gradually increased particle size, the scattering design in T2 achieved a better combination of scattering coefficient and angle.

Although multi-layer structure can improve the red light absorption while keeping efficient suppression of back-scattering, a considerable amount of large particles are incorporated and the total specific surface area decreases significantly. Consequently, the light harvesting enhancement by scattering is partially offset due to the reduction of dye. In order to avoid or reduce the decline of specific surface area, mesoporous spherical TiO_2 with high specific surface area have been synthesized by researchers.[34–37] We assume that the scattering cross-section and angle distribution of mesoporous TiO_2 sphere are same as that of TiO_2 sphere with smooth surface. By artificially raising the surface area value set in the program, the characteristics of photoelectrode films with mesoporous spheres can be simulated. For example, if the surface area of large particles in T2 increased by 10-fold (sample T2′) or 20-fold (sample T2″), the η_{LHE} and *J*sc would be improved dramatically (see Fig. 8 and Table III).

D. Comparison with reported experimental results

The influence of photoelectrode morphology on the energy conversion efficiency of N719 dye-sensitized solar cells has been investigated by Wang *et al.*[10] In their research, DSCs with photoelectrode films of different structures have been prepared, and the photocurrent action spectra as well as current-voltage curves have been tested. They have found that as tuning the film structure from monolayer to multi-layer, both the light absorption and the performance of solar cell were improved significantly. Their experimental results are in good qualitative and quantitative agreement with our simulation ones as shown above, which verifies the reliability and validity of this simulation method. However, the large TiO_2 particles used in their experiments were 50 nm and 100 nm in diameter, while the optimum size of scattering particles is 250 nm–400 nm according to our study and the experimental results reported by other researchers.[6,7,38,39] We believe that such a large deviation is mainly due to the method used by Wang *et al.* which might lead to underestimation of particle size. According to their paper, the average diameter of TiO_2 particles was calculated from the Brunauer-Emmett-Teller (BET) surface area. In fact, BET method is only suitable for particles with smooth surface. If the particle surface is rough, its size obtained by this method would be underestimated. More accurate particle size should be determined by microscopic measurement such as scanning electron microscope (SEM) or transmission electron microscope (TEM).

Chiba *et al.* have introduced the concept of haze (the ratio of diffused transmittance to total optical transmittance) to estimate the effectiveness of TiO_2 photoelectrode.[11] By controlling the addition of 400 nm particles in the film, they prepared photoelectrodes with different haze values and found that high haze in infrared region was important for advancing the IPCE and *J*sc of black dye-sensitized solar cells. In the simulation, theoretical haze can be obtained by making statistics on the final scattering angle of photons transmitted through the unsensitized TiO_2 films. Here, haze is determined as the proportion of photons with final scattering angle above 10°. Figure 9 depicts the η_{LHE} and haze values at $\lambda = 700$ nm for photoelectrodes with different structures. The film thickness is fixed as 15 μm, and the diameter of scattering particles is 400 nm. Apparently, η_{LHE} increases with haze, which is consisted with the experimental results reported by Chiba *et al.* We have also found that when the wavelength is shorter than 650 nm, the regular change of η_{LHE} with haze disappeared (not shown) either because of the strong absorption or the light loss caused by back-scattering. Therefore, haze can only be used to judge the light harvesting efficiency in the wavelength region where molar extinction coefficient of dye molecule is low and impact-III is dominant. It should be noted that the numerical relation between haze and η_{LHE} might change with material properties, film structure, preparation method, and wavelength. In our simulation, we assumed that the TiO_2 particles were spherical in shape and neglected the specular reflectance arising from the interface. These assumption and simplification might cause the simulation results to deviate from the experimental ones.

In this paper, N719 dye is chosen as the sensitizer in consideration of its wide use and to facilitate the comparison with reported experimental results. In fact, this simulation approach can be used for other sensitizers, such as black dye, organic dye, and quantum dot, or their combinations. TiO_2 can also be replaced by other kinds of materials. As shown above, this simulation approach enables us to quantitatively analyze the optical properties of photoelectrode, including

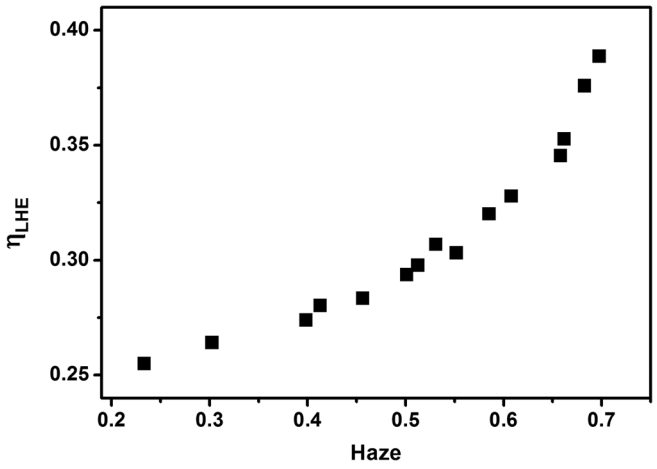

FIG. 9. Dependence of light harvesting efficiency (η_{LHE}) on haze of photoelectrode films. Both η_{LHE} and haze are calculated at $\lambda = 700$ nm. The films are of single-, double-, and multi-layer structures with various concentrations of 400 nm scattering particles.

light loss from back-scattering, average optical path length, light absorptance profile, and scattering angle. These calculated results can provide theoretical guidance for film design and optimization.

IV. CONCLUSION

In this paper, light scattering design of N719 dye-sensitized solar cells is investigated and optimized based on theoretical simulations. Submicron particles incorporated in the photoelectrode films have both positive and negative impacts on the η_{LHE} of solar cell. Therefore, the optimal scattering design should improve the light absorption in long wavelength region and suppress the light loss due to back-scattering simultaneously, which can be achieved by multi-layer structures with increased scattering coefficient. According to the simulation results, multi-layer film with gradually increased particle size demonstrates better performance. η_{LHE} can be further improved using mesoporous spherical TiO_2 with high specific surface area. The calculated results herein are in good agreement with the reported experimental ones, proving the reliability and validity of our simulation approach. As an efficient and flexible tool, this simulation approach would be useful in film design or optimization and could be a routine procedure before practice experiments.

ACKNOWLEDGMENTS

This work was supported by National Major Basic Research Project (2012CB934302), Natural Science Foundation of China (11174202, 11204176, and 61234005), and China Postdoctoral Science Foundation (2012M520889).

[1]B. O'Regan and M. Grätzel, Nature **353**, 737 (1991).
[2]M. Grätzel, J. Photochem. Photobiol., A **164**, 3 (2004).
[3]A. J. Frank, N. Kopidakis, and J. van de Lagemaat, Coord. Chem. Rev. **248**, 1165 (2004).
[4]A. Hagfeldt, G. Boschloo, L. Sun, L. Kloo, and H. Pettersson, Chem. Rev. **110**, 6595 (2010).
[5]M. K. Nazeeruddin, S. M. Zakeeruddin, R. Humphry-Baker, M. Jirousek, P. Liska, N. Vlachopoulos, V. Shklover, C.-H. Fischer, and M. Grätzel, Inorg. Chem. **38**, 6298 (1999).
[6]A. Usami, Chem. Phys. Lett. **277**, 105 (1997).
[7]J. Ferber and J. Luther, Sol. Energy Mater. Sol. Cells **54**, 265 (1998).
[8]S. Hore, C. Vetter, R. Kern, H. Smit, and A. Hinsch, Sol. Energy Mater. Sol. Cells **90**, 1176 (2006).
[9]L. Hu, S. Dai, J. Weng, S. Xiao, Y. Sui, Y. Huang, S. Chen, F. Kong, X. Pan, L. Liang, and K. Wang, J. Phys. Chem. B **111**, 358 (2007).
[10]Z. Wang, H. Kawauchi, T. Kashima, and H. Arakawa, Coord. Chem. Rev. **248**, 1381 (2004).
[11]Y. Chiba, A. Islam, R. Komiya, N. Koide, and L. Han, Appl. Phys. Lett. **88**, 223505 (2006).
[12]Y. Chiba, A. Islam, Y. Watanabe, R. Komiya, N. Koide, and L. Han, Jpn. J. Appl. Phys., Part 1 **45**, 638 (2006).
[13]F. Gao, Y. Wang, D. Shi, J. Zhang, M. Wang, X. Jing, R. H. Baker, P. Wang, S. M. Zakeeruddin, and M. Grätzel, J. Am. Chem. Soc. **130**, 10720 (2008).
[14]Y. Cao, Y. Bai, Q. Yu, Y. Cheng, S. Liu, D. Shi, F. Gao, and P. Wang, J. Phys. Chem. C **113**, 6290 (2009).
[15]A. Yella, H.-W. Lee, H. N. Tsao, C. Yi, A. K. Chandiran, M. K. Nazeeruddin, E. W.-G. Diau, C.-Y. Yeh, S. M. Zakeeruddin, and M. Grätzel, Science **334**, 629 (2011).
[16]A. Usami, Sol. Energy Mater. Sol. Cells **64**, 73 (2000).
[17]F. E. Gálvez, E. Kemppainen, H. Míguez, and J. Halme, J. Phys. Chem. C **116**, 11426 (2012).
[18]G. Rothenberger, P. Comte, and M. Grätzel, Sol. Energy Mater. Sol. Cells **58**, 321 (1999).
[19]G. A. Niklasson, C. G. Granqvist, and O. Hunderi, Appl. Opt. **20**, 26 (1981).
[20]See supplementary material at http://dx.doi.org/10.1063/1.4818438 for the evidence to support that the specular reflection at the interfaces can be omitted without influencing the optimization of scattering structure.
[21]X. Guo, Y. Zhang, D. Qin, Y. Pang, and Q. Meng, J. Power Sources **195**, 7684 (2010).
[22]X. Guo, Y. Luo, C. Li, D. Qin, D. Li, and Q. Meng, Curr. Appl. Phys. **12**, e54 (2012).
[23]M. Grätzel, Inorg. Chem. **44**, 6841 (2005).
[24]Y. Tachibana, H. Hara, K. Sayama, and H. Arakawa, Chem. Mater. **14**, 2527 (2002).
[25]R. Katoh, A. Furube, T. Yoshihara, K. Hara, G. Fujihashi, S. Takano, S. Murata, H. Arakawa, and M. Tachiya, J. Phys. Chem. B **108**, 4818 (2004).
[26]R. Katoh, A. Huijser, K. Hara, T. J. Savenije, and L. D. A. Siebbeles, J. Phys. Chem. C **111**, 10741 (2007).
[27]S. Södergren, A. Hagfeldt, J. Olsson, and S. Lindquist, J. Phys. Chem. **98**, 5552 (1994).
[28]J. Halme, K. Miettunen, and P. Lund, J. Phys. Chem. C **112**, 20491 (2008).
[29]H. K. Dunn and L. M. Peter, J. Phys. Chem. C **113**, 4726 (2009).
[30]H. Wang and L. M. Peter, J. Phys. Chem. C **113**, 18125 (2009).
[31]J. R. Jennings, F. Li, and Q. Wang, J. Phys. Chem. C **114**, 14665 (2010).
[32]J. Villanueva-Cab, H. Wang, G. Oskam, and L. M. Peter, J. Phys. Chem. Lett. **1**, 748 (2010).
[33]P. R. F. Barnes and B. C. O'Regan, J. Phys. Chem. C **114**, 19134 (2010).
[34]D. Chen, F. Huang, Y.-B. Cheng, and R. A. Caruso, Adv. Mater. **21**, 2206 (2009).
[35]D. Chen, L. Cao, F. Huang, P. Imperia, Y.-B. Cheng, and R. A. Caruso, J. Am. Chem. Soc. **132**, 4438 (2010).
[36]K. Yan, Y. Qiu, W. Chen, M. Zhang, and S. Yang, Energy Environ. Sci. **4**, 2168 (2011).
[37]D. Chen and R. A. Caruso, Adv. Funct. Mater. **23**, 1356 (2013).
[38]H.-J. Koo, J. Park, B. Yoo, K. Yoo, K. Kim, and N.-G. Park, Inorg. Chim. Acta **361**, 677 (2008).
[39]I. G. Yu, Y. J. Kim, H. J. Kim, C. Lee, and W. I. Lee, J. Mater. Chem. **21**, 532 (2011).